Nonlinear Analysis: Real World Applications 13 (2012) 2240–2258

Contents lists available at SciVerse ScienceDirect

Nonlinear Analysis: Real World Applications

journal homepage: www.elsevier.com/locate/nonrwa

Complex dynamics of a reaction–diffusion epidemic model

Weiming Wang [a,*], Yongli Cai [a], Mingjiang Wu [b], Kaifa Wang [c], Zhenqing Li [d]

[a] College of Mathematics and Information Science, Wenzhou University, Wenzhou, 325035, PR China

[b] College of Life and Environmental Science, Wenzhou University, Wenzhou, 325035, PR China

[c] Department of Medical Device and Equipment, School of Biomedical Engineering and Medical Imaging, Third Military Medical University, Chongqing 400038, PR China

[d] Laboratory of Quantitative Vegetation Ecology, Institute of Botany, The Chinese Academy of Sciences, Beijing 100093, PR China

ARTICLE INFO

Article history:
Received 17 March 2011
Accepted 20 January 2012

Keywords:
Globally asymptotically stable
Turing instability
Pattern formation

ABSTRACT

In this paper, we investigate the complex dynamics of a reaction–diffusion $S - I$ model incorporating demographic and epidemiological processes with zero-flux boundary conditions. By the method of Lyapunov function, the global stability of the disease free equilibrium and the epidemic equilibrium was established. In addition, the conditions of Turing instability were obtained and the Turing space in the parameters space were given. Based on these results, we present the evolutionary processes that involves organism distribution and their interaction of spatially distributed population with local diffusion, and find that the model dynamics exhibits a diffusion-controlled formation growth to "holes, holes–stripes, stripes, spots–stripes and spots" pattern replication. Furthermore, we indicate that the diseases' spread is getting smaller with R_0 increasing, and the increasing the diffusion of infectious will increase the speed of diseases spreading. Our results indicate that the diffusion has a great influence on the spread of the epidemic and extend well the finding of spatiotemporal dynamics in the epidemic model.

1. Introduction

Since the pioneering work of Kermack and McKendrick [1], epidemic dynamics has been an important method in analyzing the spread and control of infectious diseases qualitatively and quantitatively. The research results are helpful to predict the developing tendency of infectious diseases, to determine the key factors of the spread of infectious disease and to seek the optimum strategies of preventing and controlling the spread of infectious diseases [2]. Over a period of time, researches in theoretical and mathematical epidemiology have proposed many epidemic models and much work have been devoted to investigation the mechanism of disease transmission [3–12]. So far, the ordinary differential equations (ODEs) have been investigated by many authors in either qualitative or numerical analysis, and lots of interesting phenomena, such as stable limit cycles, periodic oscillations, bifurcations, the global asymptotic stability of the equilibria of the model and the effects of time delays, have been uncovered and we refer interested readers to more detailed discussions in [2].

The goal of the ODEs is, briefly, the quantification of the interaction within and between species and their inorganic environment, and the investigation of the temporal variation of groups of individuals of various species. It's worthy to note that the environmental factors considered in ODEs are homogeneous. While spatial variation is usually ignored, it is nevertheless true that time and space are inseparable "sister coordinates", and when populations are considered with time and space the ecological situation can be well understood [13].

* Corresponding author.
E-mail address: weimingwang2003@163.com (W. Wang).

1468-1218/$ – see front matter
doi:10.1016/j.nonrwa.2012.01.018

It is well known that the spatial component of ecological interactions has been identified as an important factor in how ecological communities are functioning and shaped, yet understanding the role of space is challenging both theoretically and empirically [13–17]. There has been a growing awareness of the importance of including a spatial aspect when constructing realistic models of biological systems, with a consequent development of both approximate and mathematical rigorous methods of analysis [18]. More recently, many studies, e.g., Refs. [19–37] and the references therein, show that the spatial epidemic model is an appropriate tool for investigating the fundamental mechanism of complex spatiotemporal epidemic dynamics. Of them, Hosono and Ilyas [19] investigated the existence of traveling wave solutions for the infective-susceptible two-component epidemic model. Cruickshank et al. [20] reported the development of a highly efficient numerical method for determining the principal characteristics (velocity, leading edge width, and peak height) of spatial invasions or epidemics described by deterministic one-dimensional reaction–diffusion models whose dynamics include the Allee effect. Ferguson et al. [21] presented an analysis of the current foot-and-mouth disease epidemic in Britain over the first 2 months of the spread of the virus, and the net transmission potential of the pathogen and the increasing impact of control measures were estimated over the course of the epidemic to date. Grenfell et al. [22] demonstrated recurrent epidemic traveling waves in an exhaustive spatiotemporal data set for measles in England and Wales. Filipe and Maule [26] investigated the effect of different spatial dispersal mechanisms on the spatiotemporal spread of disease epidemics by simulating a stochastic Susceptible-infective model motivated by previous data analysis. Mulone et al. [30] considered an epidemic model where the diffusion of individuals is influenced by intraspecific competition pressure and are weakly affected by different classes. Wang and Wang [32], Wang et al. [33], Xu and Ma [36] studied the complex dynamics of a spatial HBV model.

Besides, there have been studies of pattern formation in the spatial epidemic model, starting with the pioneering work of Turing [38]. Turing's revolutionary idea was that passive diffusion could interact with the chemical reaction in such a way that even if the reaction by itself has no symmetry-breaking capabilities, diffusion can destabilize the symmetry so that the system with diffusion can have them. Spatial epidemiology with self-diffusion has become a principal scientific discipline aiming at understanding the causes and consequences of spatial heterogeneity in disease transmission.

For example, Liu and Jin [39] addressed the question of how population diffusion affects the formation of the spatial patterns in the spatial epidemic model due to Turing mechanisms. They observed only striking formation of spatial patterns during the evolution, but the isolated ordered spot patterns do not emerge in the space. With the modified model of Liu's [39], Sun et al. [40] studied the spatiotemporal complexity of a spatial epidemic model with nonlinear incidence rate and found not only stripes and spots–stripes patterns but also spot pattern. Furthermore, Sun et al. gave a numerical study of pattern formation in the epidemic model with self and cross-diffusion and found that the model exhibits the stripes, stripes–spots and chaotic pattern [41,42]. Cai and Wang [43] investigate the complex dynamics of a reaction–diffusion $S-I-R$ model with nonlinear incidence rate of saturated mass action under zero-flux boundary conditions and found that the model dynamics exhibits a diffusion-controlled formation growth to spots, stripes–spots, stripes, stripes–holes and holes pattern replication. Furthermore, we indicated that the speed of disease spreading is getting bigger with the diffusion of infection increasing. Wang et al. [44] presented Turing pattern selection in a spatial epidemic model with cross-diffusion, derived amplitude equations for the excited modes, and found that the model dynamics exhibits complex pattern replication. Bendahmane and Saad [45] proved the weak and the global existence results of the solutions for the considered reaction–diffusion epidemic system with Neumann boundary and gave the Turing formulation via numerical simulations.

In this paper, we will focus on the spatial complex dynamics in a simple reaction–diffusion epidemic model based on the foregoing discussions. The organization of the paper is as follows. In the next section, we introduce the two-dimensional epidemic model and discuss the existence of the equilibria and the boundedness, dissipation and persistence of the solutions of the model. Furthermore, the conditions of the local and global of the equilibria and Turing bifurcation of the model are derived. In Section 3, by performing a series of simulations, we summarize and illustrate the emergence of Turing patterns. In Section 4, we give some discussions about the disease spreading with the diffusion-varying. Finally, conclusions and remarks are presented in Section 5.

2. The model and mathematical analysis

2.1. The model

In [9], Berezovsky and co-workers introduced a simple epidemic model through the incorporation of variable population, disease induced mortality, and emigration into the classical model of Kermak and McKendrick [1]. The total population (N) is divided into two groups of susceptible (S) and infectious (I), i.e., $N = S + I$. The model describing the relations between the state variables is:

$$\begin{aligned} \frac{dS}{dt} &= rN\left(1-\frac{N}{K}\right) - \beta\frac{SI}{N} - (\mu+m)S, \\ \frac{dI}{dt} &= \beta\frac{SI}{N} - (\mu+d)I, \end{aligned} \tag{1}$$

where the reproduction of susceptibles follows a logistic equation with the intrinsic growth rate r and the carrying capacity K; β denotes the contact transmission rate (the infection rate constant); μ is the natural mortality; d denotes the disease-induced mortality; m is the per-capita emigration rate of uninfectives.

For model (1), the epidemic threshold, the so-called basic reproduction number R_0 is then computed as

$$R_0 = \frac{\beta}{\mu + d}. \tag{2}$$

In epidemiology, the basic reproduction number (sometimes called basic reproductive rate or basic reproductive ratio) R_0 of an infection is the mean number of secondary cases a typical single infected case will cause in a population with no immunity to the disease in the absence of interventions to control the infection. This metric is useful because it helps determine whether or not an infectious disease will become endemic in the susceptible population. The disease will successfully invade when $R_0 > 1$ but will die out if $R_0 < 1$. $R_0 = 1$ is usually a threshold whether the disease go to extinction or go to an endemic. Large values of R_0 may indicate the possibility of a major epidemic [2]. Generally, the larger the value of R_0, the harder it is to control the epidemic. In particular, the proportion of the population that needs to be vaccinated to provide herd immunity and prevent sustained spread of the infection is given by $1 - \frac{1}{R0}$. The basic reproductive rate is affected by several factors including the duration of infectivity of affected patients, the infectiousness of the organism, and the number of susceptible people in the population that the affected patients are in contact with.

The concepts of basic demographic reproductive number R_d, which is given by

$$R_d = \frac{r}{\mu + m}. \tag{3}$$

It can be shown that if $R_d > 1$ the population grows, while $R_d \leq 1$ implies that the population does not survive.

For simplicity, re-scaling the model (1) by letting $S \to S/K, I \to I/K, t \to t/(\mu + d)$ leads to the following model

$$\begin{aligned} \frac{dS}{dt} &= \nu R_d(S + I)(1 - (S + I)) - R_0 \frac{SI}{S + I} - \nu S \triangleq f(S, I), \\ \frac{dI}{dt} &= R_0 \frac{SI}{S + I} - I \triangleq g(S, I), \end{aligned} \tag{4}$$

where $\nu = \frac{\mu+m}{\mu+d}$ is defined by the ratio of the average life-span of susceptibles to that of infections.

For details, we refer to the reader Section 2 in the Ref. [9].

The simple models (e.g., model (4)) we have described so far assume that the susceptible S and infectious I experience the same homogeneous environment. In reality, individual organisms are distributed in space and typically interact with the physical environment and other organisms in their spatial neighborhood. Many physical aspects of the environment such as climate, chemical composition, or physical structure can vary from place to place. And there is considerable evidence that space can affect the dynamics of populations and the structure of communities. There are some biological phenomena, such as invasions by exotic species, which are intrinsically spatial in nature and thus require models that involve space. One of the main reasons why many species are threatened or endangered is the destruction or fragmentation of their habitats. The goal of understanding how patterns of habitat destruction and fragmentation affect the persistence of populations provides a strong motivation to develop models for spatial effects [15].

Based on the above discussions, assuming that the susceptible (S) and infectious (I) population move randomly—described as Brownian random motion [17], then we propose a simple spatial model corresponding to (4) as follows:

$$\begin{aligned} \frac{\partial S}{\partial t} &= \nu R_d(S + I)\,(1 - (S + I)) - R_0 \frac{SI}{S + I} - \nu S + d_1 \nabla^2 S, \\ \frac{\partial I}{\partial t} &= R_0 \frac{SI}{S + I} - I + d_2 \nabla^2 I \end{aligned} \tag{5}$$

where the nonnegative constants d_1 and d_2 are the diffusion coefficients of S and I, respectively. $\nabla^2 = \frac{\partial^2}{\partial x^2} + \frac{\partial^2}{\partial y^2}$, the usual Laplacian operator in two-dimensional space, is used to describe the Brownian random motion.

Usually for the spatial spread of infectious disease is studied by analyzing traveling wave solutions and calculating its minimal wave speed. In this paper, we will study the complex dynamics of the spatial transitions through analysis of Turing instability and Turing patterns for model (5).

Model (5) is to be analyzed under the following non-zero initial conditions

$$S(\mathbf{r}, 0) = S_0(\mathbf{r}) \geq 0, \qquad I(\mathbf{r}, 0) = I_0(\mathbf{r}) \geq 0, \quad \mathbf{r} = (x, y) \in \Omega = [0, L] \times [0, L], \tag{6}$$

and zero-flux boundary conditions:

$$\frac{\partial S}{\partial n} = \frac{\partial I}{\partial n} = 0. \tag{7}$$

In the above, n is the outward unit normal vector of the boundary $\partial\Omega$ which we assume is smooth. The main reason for choosing such boundary conditions is that we are interested in the self-organization of patterns. Zero-flux boundary conditions imply that the domain of model boundary is simply reflective, and that the domain is isolated or insulated from the external environment [46]. The zero-flux conditions imply that there are no fluxes of populations through the boundary, i.e., no external input is imposed from outside [16].

2.2. The boundedness of the non-spatial model

In this subsection, we investigate some preliminary but relevant properties of the dynamical model (4). The first one concerns the existence of the solutions.

Theorem 2.1. *All the non-negative solutions of model (4) that start in $\Re^+$ are bounded, with ultimate bound $\boldsymbol{\Gamma}$ independent of the initial conditions.*

Proof. Summing up the two equations in model (4) and denoting $W(t) = S(t) + I(t)$, we have

$$\frac{dW}{dt} = \nu R_d(S+I)(1-(S+I)) - \nu S - I.$$

For each $\eta > 0$, the following inequalities hold:

$$\begin{aligned}\frac{dW}{dt} + \eta W &= \nu R_d(S+I-(S+I)^2) - (\nu-\eta)S - (1-\eta)I \\ &\le \nu R_d(W - W^2) - (\nu-\eta)S - (1-\eta)I.\end{aligned}$$

Take $\eta < \min\{\nu R_d,\ \nu,\ 1\}$, then the right-hand side of the above inequality is bounded. That is,

$$\frac{dW}{dt} + \eta W \le \nu R_d(W - W^2).$$

From the above equation, we have $\frac{dW}{dt} \le (\nu R_d - \eta - \nu R_d W)W$. There exists a T, such that for $t > T$,

$$\limsup_{t\to\infty} W(t) \le 1 - \frac{\eta}{\nu R_d} \triangleq \boldsymbol{\Gamma}.$$

It is easy to see that $\boldsymbol{\Gamma}$ is independent of the initial condition. We conclude the proof. □

Remark 2.2. The feasible domain for model (4) is the triangular region inside $0 < S + I \le 1 - \frac{\eta}{\nu R_d}$, which is more exact than the result $0 < S + I \le 1$ in [9,47].

2.3. The equilibria

It is not difficult to see that model (4) always has a disease free equilibrium $E_0 = (S_0, I_0) = \left(1 - \frac{1}{R_d}, 0\right)$ for $R_d > 1$. Further, if $R_d > \frac{1}{R_0}$ and $R_d > \frac{R_0+\nu-1}{\nu R_0} \triangleq R_d^+$, $R_0 > 1$ hold, then model (4) has an endemic equilibrium $E^* = (S^*, I^*)$ which is given by

$$\begin{aligned}S^* &= \frac{\nu R_0 R_d - R_0 + 1 - \nu}{\nu R_0^2 R_d}, \\ I^* &= (R_0 - 1)\frac{\nu R_0 R_d - R_0 + 1 - \nu}{\nu R_0^2 R_d} = (R_0 - 1)S^*.\end{aligned} \tag{8}$$

The Jacobian matrix of model (4) at the disease-free equilibrium $E_0 = (S_0, I_0)$ is

$$A = \begin{pmatrix} \nu(1-R_d) & \nu(2-R_d) - R_0 \\ 0 & R_0 - 1 \end{pmatrix}.$$

A has negative eigenvalues, implying the asymptotic stability of the disease-free equilibrium, provided $R_0 < 1$, in this case, model (4) has a unique equilibrium $E_0 = (S_0, I_0)$. So, we have:

Lemma 2.3. *Suppose $R_d > 1$, if $R_0 < 1$, the equilibrium $E_0 = (S_0, I_0)$ of model (4) is a stable node, while $R_0 > 1$, E_0 is a saddle.*

The Jacobian of model (4) around the endemic $E^* = (S^*, I^*)$ is given by

$$J = \begin{pmatrix} -\dfrac{R_0^2 + \nu R_0 R_d + \nu R_0 - 4R_0 - 2\nu + 3}{R_0} & \dfrac{2R_0 + 2\nu - \nu R_0 R_d - 3}{R_0} \\ \dfrac{(R_0-1)^2}{R_0} & \dfrac{1}{R_0} - 1 \end{pmatrix} \triangleq \begin{pmatrix} a_{11} & a_{12} \\ a_{21} & a_{22} \end{pmatrix}. \tag{9}$$

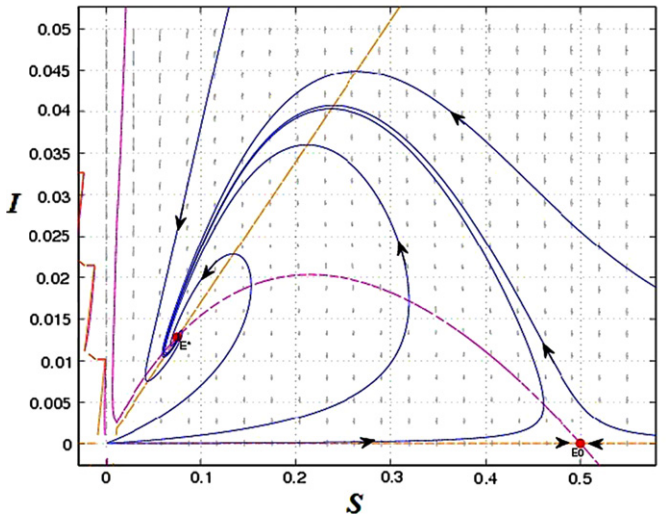

Fig. 1. Phase portrait of (4) with $R_0 = 1.17$, $R_d = 2$ and $\nu = 0.15$. The horizontal axis is the susceptible population S, and the vertical axis is the infected population I. The dashed curve is the S-nullcline, and the dashed-dotted vertical line is the I-nullcline. The equilibrium $E_0 = (0.5, 0)$ is a saddle and $E^* = (0.0754864, 0.0128327)$ is locally asymptotically stable.

Obviously, if E^* exists, i.e., $R_d > \frac{R_0+\nu-1}{\nu R_0}$ and $R_0 > 1$ hold, then one can get:

$$\begin{aligned} \det(J) &= a_{11}a_{22} - a_{12}a_{21} = \frac{(\nu R_0 R_d - R_0 + 1 - \nu)(R_0 - 1)}{R_0} > 0, \\ \operatorname{tr}(J) &= a_{11} + a_{22} = -\frac{\nu R_0 R_d - R_0 + 1 - \nu + (R_0 - 1)(R_0 - 1 + \nu)}{R_0} < 0. \end{aligned} \tag{10}$$

By Roth–Hurwitz criterion, we can get:

Lemma 2.4. *If $R_d > \frac{R_0+\nu-1}{\nu R_0}$ and $R_0 > 1$ hold, the endemic equilibrium $E^* = (S^*, I^*)$ of model (4) is always locally asymptotically stable.*

In Fig. 1, we show the phase portrait of (4) with $R_0 = 1.17$, $R_d = 2$ and $\nu = 0.15$. The horizontal axis is the susceptible population S, and the vertical axis is the infected population I. The dashed curve is the S-nullcline, and the dashed-dotted vertical line is the I-nullcline. The equilibrium $E_0 = (0.5, 0)$ is a saddle and $E^* = (0.0754864, 0.0128327)$ is locally asymptotically stable.

2.4. Some preliminary properties of the spatial model

2.4.1. Dissipation

Theorem 2.5. *For any solution $(S(\mathbf{r}, t), I(\mathbf{r}, t))$ of model (5) with nonnegative initial conditions (6), if $R_0 > 1$, then:*

$$\limsup_{t\to\infty} \max_{\bar{\Omega}} S(\mathbf{r}, t) \le \frac{1}{4} R_d, \qquad \limsup_{t\to\infty} \max_{\bar{\Omega}} I(\mathbf{r}, t) \le \frac{1}{4} R_d (R_0 - 1).$$

Hence, for any $\varepsilon > 0$, the rectangle $[0, \frac{1}{4}R_d + \varepsilon] \times [0, \frac{1}{4}R_d(R_0 - 1) + \varepsilon]$ is a global attractor of model (5) in $\Re^+$.

Proof. Note that S satisfies

$$\begin{cases} \dfrac{\partial S}{\partial t} - d_1 \nabla^2 S \le \dfrac{1}{4}\nu R_d - \nu S, & \mathbf{r} \in \Omega, t > 0, \\ \dfrac{\partial S}{\partial n} = 0, & \mathbf{r} \in \partial\Omega, t > 0, \\ S(\mathbf{r}, 0) = S_0(\mathbf{r}), & \mathbf{r} \in \Omega. \end{cases} \tag{11}$$

Let $Z(t)$ be a solution of the ordinary differential equation

$$\dot{Z}(t) = \frac{1}{4}\nu R_d - \nu Z \ (t \ge 0) \quad \text{with the initial condition } Z(0) = \max_{\bar{\Omega}} S(\mathbf{r}, 0) > 0.$$

Then $\lim_{t\to\infty} Z(t) = \frac{1}{4}R_d$. From the comparison principle, one can get $S(\mathbf{r}, t) \le Z(t)$, hence,

$$\limsup_{t\to\infty} \max_{\bar{\Omega}} S(\mathbf{r}, t) \le \frac{1}{4}R_d.$$

As a result, for any $\varepsilon > 0$, there exists $T > 0$, such that $S(\mathbf{r}, t) \le \frac{1}{4}R_d + \varepsilon$ for all $\mathbf{r} \in \bar{\Omega}$ and $t \ge T$. Similarly, I satisfies,

$$\begin{cases} \dfrac{\partial I}{\partial t} - d_1\nabla^2 I \le I\dfrac{R_0\left(\frac{1}{4}R_d + \varepsilon\right) - \left(\frac{1}{4}R_d + \varepsilon\right) - I}{\frac{1}{4}R_d + \varepsilon + I}, & \mathbf{r} \in \Omega, t > 0, \\ \dfrac{\partial I}{\partial n} = 0, & \mathbf{r} \in \partial\Omega, t > 0, \\ I(\mathbf{r}, 0) = I_0(\mathbf{r}), & \mathbf{r} \in \Omega. \end{cases} \tag{12}$$

Since $R_0 > 1$, there exists $\varepsilon > 0$, such that $R_0\left(\frac{1}{4}R_d + \varepsilon\right) - \left(\frac{1}{4}R_d + \varepsilon\right) > 0$. Thus, $\limsup_{t\to\infty} \max_{\bar{\Omega}} I(\mathbf{r}, t) \le R_0\left(\frac{1}{4}R_d + \varepsilon\right) - \left(\frac{1}{4}R_d + \varepsilon\right)$. From the arbitrariness of $\varepsilon > 0$, we can get that

$$\limsup_{t\to\infty} \max_{\bar{\Omega}} I(\mathbf{r}, t) \le \frac{1}{4}R_d(R_0 - 1). \tag{13}$$

This ends the proof. □

2.4.2. Persistence

Definition 2.6 (*[48]*)**.** The spatial model (5) is said to have the persistence property if for any nonnegative initial data $\left(S_0(\mathbf{r}), I_0(\mathbf{r})\right)$, there exists a positive constant $\varepsilon = \varepsilon(S_0, I_0)$, such that the corresponding solution, (S, I) of model (5) satisfies

$$\liminf_{t\to\infty} \min_{\bar{\Omega}} S(\mathbf{r}, t) \ge \varepsilon, \qquad \liminf_{t\to\infty} \min_{\bar{\Omega}} I(\mathbf{r}, t) \ge \varepsilon. \tag{14}$$

Theorem 2.7. *If $R_d > 1 + \frac{1}{\nu}$ and $1 < R_0 < \frac{\nu(R_d^2 + 2R_d - 2)}{\nu R_d^2 + 2}$, then model (5) has the persistence property.*

Proof. The proof is based on comparison principles. From (13), for $0 < \varepsilon \ll 1$, it is clear that there exists a $t \gg 1$, such that $I(\mathbf{r}, t) < \frac{1}{4}R_d(R_0 - 1) + \varepsilon \triangleq \alpha$ for all $\mathbf{r} \in \bar{\Omega}$ and $t \ge t_0$. Hence, $S(\mathbf{r}, t)$ is an upper solution of the following problem:

$$\begin{cases} \dfrac{\partial z}{\partial t} - d_1\nabla^2 z = z(\nu R_d - 2\alpha\nu R_d - R_0 - \nu - \nu R_d z), & \mathbf{r} \in \Omega, t > t_0, \\ \dfrac{\partial z}{\partial n} = 0, & \mathbf{r} \in \partial\Omega, t > t_0, \\ z(\mathbf{r}, t_0) = S_0(\mathbf{r}, t_0) \ge 0, & \mathbf{r} \in \bar{\Omega}. \end{cases} \tag{15}$$

Let $S(t)$ be the unique positive solution to the following problem:

$$\begin{cases} \dfrac{dw}{dt} = w(\nu R_d - 2\alpha\nu R_d - R_0 - \nu - \nu R_d w), & t > t_0, \\ w(t_0) = \max\limits_{\bar{\Omega}} S_0(\mathbf{r}, t_0) \ge 0. \end{cases} \tag{16}$$

Since $R_d > 1 + \frac{1}{\nu}$ and $1 < R_0 < \frac{\nu(R_d^2 + 2R_d - 2)}{\nu R_d^2 + 2}$, there exist ε such that $\nu R_d - 2\alpha\nu R_d - R_0 - \nu > 0$, then $\lim_{t\to\infty} w(t) = \frac{\nu R_d - \frac{1}{2}\nu R_d^2(R_0 - 1) - R_0 - \nu}{\nu R_d} \triangleq \widehat{w}$. By comparison, it follows that $\lim_{t\to\infty} S(\mathbf{r}, t) = \widehat{w}$. This implies

$$\liminf_{t\to\infty} \min_{\bar{\Omega}} S(\mathbf{r}, t) \ge \widehat{w}. \tag{17}$$

Hence, $S(\mathbf{r}, t) > \widehat{w} - \varepsilon$ for $t > t_0$ and $\mathbf{r} \in \bar{\Omega}$.

Similarly, by the second equation in model (5), we have that $I(\mathbf{r}, t)$ is an upper solution of problem:

$$\begin{cases} \dfrac{\partial z}{\partial t} - d_1\nabla^2 z = z\dfrac{\widehat{w}(R_0 - 1) - (R_0 - 1)\varepsilon - z}{\widehat{w} - \varepsilon + z}, & \mathbf{r} \in \Omega, t > t_0, \\ \dfrac{\partial z}{\partial n} = 0, & \mathbf{r} \in \partial\Omega, t > t_0, \\ z(\mathbf{r}, t_0) = I_0(\mathbf{r}) \ge 0, & \mathbf{r} \in \bar{\Omega}. \end{cases} \tag{18}$$

Let $I(t)$ be the unique positive solution to the following problem:

$$\begin{cases} \dfrac{dw}{dt} = w\dfrac{\widehat{w}(R_0-1)-(R_0-1)\varepsilon - w}{\widehat{w}-\varepsilon+w}, & t > t_0, \\ w(t_0) = \max\limits_{\bar{\Omega}} I_0(\mathbf{r}, t_0) \geq 0. \end{cases} \tag{19}$$

Then $\lim_{t\to\infty} w(t) = \widehat{w}(R_0-1)$ for the arbitrariness of ε, and an application of the comparison principle gives

$$\liminf_{t\to\infty} \min_{\bar{\Omega}} I(\mathbf{r}, t) \geq \widehat{w}(R_0-1). \tag{20}$$

The proof is complete. □

2.5. The stability of the equilibria of the spatial model

In this subsection, we will analyze the local and global stability of the disease free equilibrium $E_0 = (S_0, I_0)$ and the endemic equilibrium $E^* = (S^*, I^*)$ of model (5).

Let $0 = \mu_0 < \mu_1 < \mu_2 < \cdots$ be the eigenvalues of the operator-∇^2 on Ω with the homogeneous zero-flux boundary condition. Set

$$\mathbf{X} = \left\{ (S, I) \in [C^1(\bar{\Omega})]^2 \;\middle|\; \frac{\partial S}{\partial n} = \frac{\partial I}{\partial n} = 0 \text{ on } \partial\Omega \right\}$$

and consider the decomposition $\mathbf{X} = \bigoplus_{i=0}^{\infty} \mathbf{X}_i$, where $\mathbf{X}_i$ is the eigenspace corresponding to μ_i.

Theorem 2.8. (T1) *If $R_0 < 1$, then the disease free equilibrium E_0 of model (5) is uniformly asymptotically stable.*
(T2) *If either of the following inequalities holds:*
(a) $\nu > \frac{(R_0-1)(3-R_0)}{R_0-2+R_0R_d}$, *when* $R_d > \frac{1}{R_0(2-R_0)}$ *and* $1 < R_0 < 2$,
(b) $\nu > \frac{R_0-1}{R_0R_d-1}$, *when* $R_d > \frac{1}{R_0}$ *and* $2 < R_0 < 3$,

then the endemic equilibrium E^* of model (5) is uniformly asymptotically stable.

Proof. We only prove (T2). (T1) can be established in a similar manner as (T2).

The linearization of (5) at the positive equilibrium E^* is

$$\frac{\partial}{\partial t}\begin{pmatrix} S \\ I \end{pmatrix} = \pounds \begin{pmatrix} S \\ I \end{pmatrix} + \begin{pmatrix} f_1(S-S^*, I-I^*) \\ f_2(S-S^*, I-I^*) \end{pmatrix},$$

where $f_i(z_1, z_2) = O(z_1^2 + z_2^2)$ $(i = 1, 2)$, and

$$\pounds = \begin{pmatrix} d_1\nabla^2 + a_{11} & a_{12} \\ a_{21} & d_2\nabla^2 + a_{22} \end{pmatrix}.$$

Now, we discuss the sign of a_{11} as the following two cases.

Note that the sign of a_{11} is determined by

$$\phi = \nu(R_0R_d + R_0 - 2) + (R_0-1)(R_0-3).$$

The endemic equilibrium E^* of model (5) exists if $\nu > \frac{R_0-1}{R_0R_d-1}$ is true. Hence, we find that $\phi > 0$ holds if and only if

$$\nu > \frac{(R_0-1)(3-R_0)}{R_0R_d + R_0 - 2}.$$

Furthermore, easy computations yield

$$\frac{(R_0-1)(3-R_0)}{R_0R_d+R_0-2} - \frac{R_0-1}{R_0R_d-1} = \frac{(R_0-1)(R_0R_d(2-R_0)-1)}{(R_0R_d+R_0-2)(R_0-1)}. \tag{21}$$

If $1 < R_0 < 2$ and $R_d > \frac{1}{R_0(2-R_0)}$ hold, from (21), we can get that $\nu > \frac{(R_0-1)(3-R_0)}{R_0-2+R_0R_d}$; if $2 < R_0 < 3$ and $R_d > \frac{1}{R_0}$ hold, from (21), we can observe that $\nu > \frac{(R_0-1)}{R_0R_d-1}$.

Hence, in both cases of the assumptions of Theorem 4 (T2), we have $a_{11} < 0$. For each i $(i = 0, 1, 2, \ldots)$, $\mathbf{X}_i$ is invariant under the operator £, and £ is an eigenvalue of £ on $\mathbf{X}_i$ if and only if λ is an eigenvalue of the matrix,

$$A_i = \begin{pmatrix} -d_1\mu_i + a_{11} & a_{12} \\ a_{21} & -d_2\mu_i + a_{22} \end{pmatrix}. \tag{22}$$

Noting that

$$\begin{aligned} &\det(A_i) = d_1 d_2 \mu_i^2 - (d_1 a_{22} + d_2 a_{11})\mu_i + \det(J) > 0, \\ &\operatorname{tr}(A_i) = -(d_1 + d_2)\mu_i + \operatorname{tr}(J) < 0, \end{aligned} \tag{23}$$

where $\det(A_i)$ and $\operatorname{tr}(A_i)$ are respectively the determinant and trace of A_i. Because $\det(A_i) > 0$, $\operatorname{tr}(A_i) < 0$, the two eigenvalues λ_i^+ and λ_i^- have negative real parts. For any $i \geq 0$, the following hold:

Case 1: For $i = 0$, if $(\operatorname{tr}(J))^2 - 4\det(J) \leq 0$,

$$\operatorname{Re}(\lambda_0^{\pm}) = \frac{1}{2}\operatorname{tr}(J) < 0,$$

and if $(\operatorname{tr}(J))^2 - 4\det(J) > 0$,

$$\operatorname{Re}(\lambda_0^{+}) = \frac{\operatorname{tr}(J) + \sqrt{(\operatorname{tr}(J))^2 - 4\det(J)}}{2} < 0,$$

$$\operatorname{Re}(\lambda_0^{-}) = \frac{\operatorname{tr}(J) - \sqrt{(\operatorname{tr}(J))^2 - 4\det(J)}}{2} < 0.$$

Case 2: For $i \geq 1$, if $(\operatorname{tr}(A_i))^2 - 4\det(A_i) \leq 0$, then

$$\operatorname{Re}(\lambda_0^{\pm}) = \frac{1}{2}\operatorname{tr}(A_i) \leq \frac{1}{2}\operatorname{tr}(J) < 0,$$

if $(\operatorname{tr}(A_i))^2 - 4\det(A_i) > 0$, since $\det(A_i) > 0$ and $\operatorname{tr}(A_i) < 0$,

$$\operatorname{Re}(\lambda_i^{-}) = \frac{\operatorname{tr}(A_i) - \sqrt{(\operatorname{tr}(A_i))^2 - 4\det(A_i)}}{2} \leq \frac{1}{2}\operatorname{tr}(A_i) \leq \frac{1}{2}\operatorname{tr}(J) < 0,$$

$$\operatorname{Re}(\lambda_i^{+}) = \frac{\operatorname{tr}(A_i) + \sqrt{(\operatorname{tr}(A_i))^2 - 4\det(A_i)}}{2} = \frac{2\det(A_i)}{\operatorname{tr}(A_i) - \sqrt{(\operatorname{tr}(A_i))^2 - 4\det(A_i)}} \leq \frac{\det(A_i)}{\operatorname{tr}(A_i)} < \tilde{\delta}$$

for some positive $\tilde{\delta}$ which is independent of i.

This shows that there exists a positive constant δ, which is independent of i, such that $\operatorname{Re}(\lambda_i^{\pm}) < \delta$ for all i. Hence, the spectrum of £ which consists of eigenvalues lies on $\{\operatorname{Re}(\lambda) < \delta\}$. In the sense of [49], we have that the endemic equilibrium E^* of model (5) is uniformly asymptotically stable. The proof is complete. □

Next, we consider the global stability of the disease free equilibrium E_0 of model (5). The technique of the proof is to use the comparison arguments.

Theorem 2.9. *If $R_0 < 1$ and $R_d > 1$, then the disease free equilibrium $E_0 = (1 - \frac{1}{R_d}, 0)$ of model (5) is globally asymptotically stable.*

Proof. It suffices to prove that each positive solution $(S(\mathbf{r}, t), I(\mathbf{r}, t))$ of model (5) tends to E_0 as $t \to \infty$. This will be done $(S(\mathbf{r}, t), I(\mathbf{r}, t)) \to (1 - \frac{1}{R_d}, 0)$, uniformly on $\bar{\Omega}$ as $t \to \infty$.

Since I satisfies

$$\begin{cases} \dfrac{\partial I}{\partial t} - d_1 \nabla^2 I \leq (R_0 - 1)I, & \mathbf{r} \in \Omega, t > 0, \\ \dfrac{\partial I}{\partial n} = 0, & \mathbf{r} \in \partial\Omega, t > 0, \\ I(\mathbf{r}, 0) = I_0(\mathbf{r}) \geq 0, & \mathbf{r} \in \bar{\Omega}. \end{cases} \tag{24}$$

If $R_0 < 1$, from the simple comparison argument, there exist $0 < \varepsilon \ll 1$ and a $t_0 \gg 0$, such that $I < \varepsilon$ for all $\mathbf{r} \in \bar{\Omega}$, and $t \geq t_0$.

Since ε is arbitrary and sufficiently small, we conclude that $S(\mathbf{r}, t)$ is a lower solution of the following problem:

$$\begin{cases} \dfrac{\partial z}{\partial t} - d_1 \nabla^2 z = \nu z(R_d - 1 - R_d z), & \mathbf{r} \in \Omega, t > t_0, \\ \dfrac{\partial z}{\partial n} = 0, & \mathbf{r} \in \partial\Omega,\ t > t_0, \\ z(\mathbf{r}, t_0) = S_0(\mathbf{r}) \geq 0, & \mathbf{r} \in \bar{\Omega}. \end{cases} \tag{25}$$

Let $S(t)$ be a solution of the ordinary differential equation,

$$\begin{cases} \dfrac{dw(t)}{dt} = \nu w(R_d - 1 - R_d w), \quad t > t_0, \\ w(t_0) = \max\limits_{\bar{\Omega}} S(\mathbf{r}, t_0) > 0. \end{cases} \tag{26}$$

Then $S(\mathbf{r}, t)$ is an upper solution of the problem (25). Hence, we derive from (26) that $\lim_{t\to\infty} w(t) = 1 - \frac{1}{R_d}$. By comparison, it follows that $\lim_{t\to\infty} S(\mathbf{r}, t) = 1 - \frac{1}{R_d}$ uniformly for $\mathbf{r} \in \bar{\Omega}$.

Hence, $S(\mathbf{r}, t) \to 1 - \frac{1}{R_d}$ and $I(\mathbf{r}, t) \to 0$ uniformly on $\bar{\Omega}$ as $t \to \infty$. This shows the disease free equilibrium is globally stable. The proof is complete. □

One of the epidemiological implication of Theorem 2.9 is that the infected population vanishes in time so the disease dies out, a growing population if the disease is not endemic ($R_0 < 1$).

Next, we show the global stability behavior of the endemic equilibrium E^* for model (5). Biologically, the statement of the global stability of the endemic equilibrium E^* means that, however quickly or slowly the two individuals diffuse, the disease will spatially homogeneously exist over time.

Theorem 2.10. *If the endemic equilibrium E^* of model (5) exists, assume that any one of the following two conditions is true:*

(i) *when* $\nu > 1$, $\frac{1}{R_0} < R_d < 1$;

(ii) *when* $\nu < 1$, $R_d > \max\left\{1, \frac{2R_0 - 1 + \nu}{\nu R_0} - 1\right\}$,

the endemic equilibrium E^* of model (5) is globally asymptotically stable provided that

$$4\nu R_d S^*(1 - I^*) > \nu^2 R_d^2 + 4S^{*2}. \tag{27}$$

Proof. Define a Lyapunov function:

$$V(S, I) = \int_{S^*}^{S} \frac{\xi - S^*}{\xi} d\xi + \lambda \int_{I^*}^{I} \frac{\eta - I^*}{\eta} d\eta, \tag{28}$$

where the constant $\lambda > 0$ and will be determined later. We note that $V(S, I)$ is non-negative, $V(S, I) = 0$ if and only if $(S(\mathbf{r}, t), I(\mathbf{r}, t)) = (S^*, I^*)$. Furthermore, the time derivative of V along the solutions of (4) is

$$\frac{dV}{dt} = \frac{S - S^*}{S} \frac{dS}{dt} + \frac{\lambda(I - I^*)}{I} \frac{dI}{dt}.$$

Noting the equalities

$$\nu R_d(S^* + I^*)(1 - (S^* + I^*)) - \frac{R_0 S^* I^*}{S^* + I^*} - \nu S^* = 0, \qquad \frac{R_0 S^*}{S^* + I^*} - 1 = 0,$$

we have,

$$\begin{aligned} \frac{dV}{dt} &= (S - S^*)\left[\nu R_d\left(1 + \frac{I}{S} - S - 2I - \frac{I^2}{S}\right) - \frac{R_0 I}{S + I} - \nu R_d\left(1 + \frac{I^*}{S^*} - S^* - 2I^* - \frac{I^{*2}}{S^*}\right) + \frac{R_0 I^*}{S^* + I^*}\right] \\ &\quad + \frac{\lambda I^*(S - S^*)(I - I^*)}{S^*(S + I)} - \frac{\lambda(I - I^*)^2}{S + I} \\ &= \frac{(S - S^*)^2}{S^* S(S + I)}\left(-\nu R_d S^* S^2 - (\nu R_d(1 - I^*) - 1)I^* S - \nu R_d I(1 - I^*) - \nu R_d SI\right) \\ &\quad + (S - S^*)(I - I^*)\left(\frac{\nu R_d(S - 2SS^* - S^* I - S^* I^*)}{S^* S} - \frac{1}{S + I} + \frac{\lambda I^*}{S^*(S + I)}\right) - \frac{\lambda(I - I^*)^2}{S + I}. \end{aligned} \tag{29}$$

Hence, if we choose $\lambda = \frac{S^*}{I^*}$, then we have

$$\begin{aligned} \frac{dV}{dt} &< -\frac{(S - S^*)^2}{S^* S(S + I)}\left((\nu R_d(1 - I^*) - 1)I^* S\right) + \frac{\nu R_d(S - S^*)(I - I^*)}{S^*} - \frac{S^*(I - I^*)^2}{I^*(S + I)} \\ &= \frac{1}{S^* S(S + I)}\left(-B_1(S - S^*)^2 + B_2(S - S^*)(I - I^*) - B_3(I - I^*)^2\right), \end{aligned} \tag{30}$$

where

$$B_1 = (\nu R_d(1-I^*)-1)I^*S,$$
$$B_2 = \nu R_d S(S+I) > 0,$$
$$B_3 = \frac{S^{*2}S}{I^*} > 0.$$

In both cases of assumptions (i) and (ii), we have

$$\nu R_d(1-I^*)-1 = \frac{\nu R_0 R_d - R_0 + 1 - \nu + R_0(\nu-1)}{R_0^2} > 0,$$

which is equivalent to $B_1 > 0$.

Obviously, when $(S-S^*)(I-I^*) < 0$, then from (30), we have $\frac{dV}{dt} < 0$ is always true. When $(S-S^*)(I-I^*) > 0$, since the arithmetical mean is greater than or equal to the geometrical mean, we have $\frac{dV}{dt} < 0$ if $B_2^2 \le 4B_1B_3$, which is equivalent to

$$\Big(\nu R_d S(S+I)\Big)^2 < 4S^{*2}S^2\Big(\nu R_d(1-I^*)-1\Big). \tag{31}$$

By Theorem 2.1, it is sufficient to impose the restriction

$$\nu^2 R_d^2 < 4S^{*2}\Big(\nu R_d(1-I^*)-1\Big). \tag{32}$$

We observe that under our assumption (27) and (32) is valid, which reduces to $\frac{dV}{dt} < 0$. This means that the endemic equilibrium E^* of model (4) is globally asymptotically stable (see, Fig. 2).

Next, we select the Lyapunov function for model (5):

$$E(t) = \iint_\Omega V(S,I)dA. \tag{33}$$

So, differentiating $E(t)$ with respect to time t along the solutions of model (5), we obtain

$$\frac{dE(t)}{dt} = \iint_\Omega \frac{dV}{dt}dA + \iint_\Omega \left(\frac{\partial V}{\partial S}d_1\nabla^2 S + \frac{\partial V}{\partial I}d_2\nabla^2 I\right)dA. \tag{34}$$

Using Green's first identity in the plane, and considering the zero-flux boundary conditions (7), one can show that

$$\begin{aligned}\frac{dE(t)}{dt} &= \iint_\Omega \frac{dV}{dt}dA - \left[\frac{d_1S^*}{S^2}\iint_\Omega\left(\left(\frac{\partial S}{\partial x}\right)^2+\left(\frac{\partial S}{\partial y}\right)^2\right)dA + \frac{d_2S^*}{I^2}\iint_\Omega\left(\left(\frac{\partial I}{\partial x}\right)^2+\left(\frac{\partial I}{\partial y}\right)^2\right)dA\right]\\ &\le \iint_\Omega \frac{dV}{dt}dA \le 0.\end{aligned} \tag{35}$$

Thus, the endemic equilibrium E^* of model (5) is globally asymptotically stable. □

In Fig. 2, we show the phase portrait of (4) with a $R_0 = 1.17$, $R_d = 1.5$ and $\nu = 1.1$. In this case, the equilibrium $E_0 = (0.33333, 0)$ is a saddle and $E^* = (0.29243, 0.049713)$ is globally asymptotically stable.

2.6. Turing instability

An equilibrium is Turing instability means that it is an asymptotically stable equilibrium of model (4) but is unstable with respect to solutions of spatial model (5). Hence, Turing instability occurs when the condition either $\mathrm{tr}(A_i) < 0$ or $\det(A_i) > 0$ is violated. From the above discussion, we see that the endemic equilibrium E^* of model (4) is asymptotically stable, which implies that $\mathrm{tr}(A_i) < 0$. Therefore, in order for Turing instability, we need $\det(A_i) < 0$. This implies that the matrix A_i, and so to the operator £, has at least one positive eigenvalue. By Henry [49], it follows that the endemic equilibrium E^* of model (5) is unstable. On the other hand, since $\mu_i > 0$, a necessary condition for the instability is that $d_1a_{22} + d_2a_{11} > 0$, which is equivalent to $a_{11} > -\frac{d_1a_{22}}{d_2} > 0$. As a consequence, we know if $a_{11} > 0$, then

$$\nu < \frac{(R_0-1)(3-R_0)}{R_0R_d + R_0 - 2},$$

thus, from (21), we have $R_d > \frac{1}{R_0(2-R_0)}$ and $1 < R_0 < 2$. Summarizing the above, one can get the following theorem:

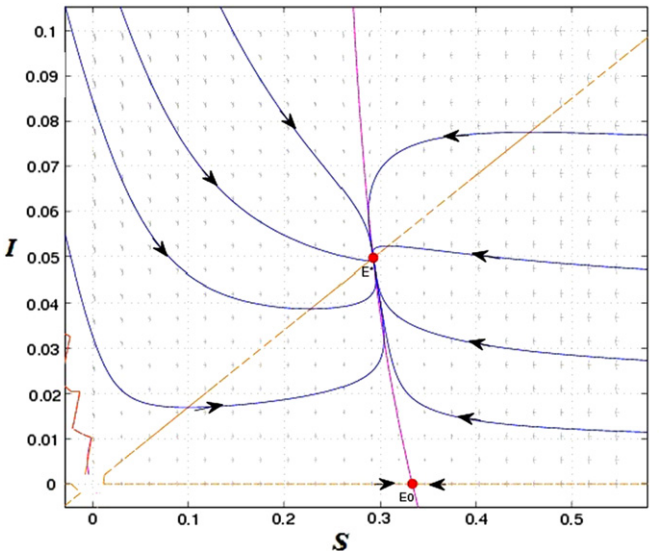

Fig. 2. Phase portrait of (4) with a $R_0 = 1.17$, $R_d = 1.5$ and $\nu = 1.1$. The horizontal axis is the susceptible population S, and the vertical axis is the infected population I. The dashed curve is the S-nullcline, and the dashed-dotted vertical line is the I-nullcline. The equilibrium $E_0 = (0.33333, 0)$ is a saddle and $E^* = (0.29243, 0.049713)$ is globally asymptotically stable.

Theorem 2.11. *When* $1 < R_0 < 2$, *if* $R_d > \frac{1}{R_0(2-R_0)}$ *and* $\frac{R_0-1}{R_0R_d-1} < \nu < \frac{(R_0-1)(3-R_0)}{R_0-2+R_0R_d}$ *hold, the endemic equilibrium* E^* *of model* (5) *is a Turing instability if the following hypotheses hold:*

(i) $d_1a_{22} + d_2a_{11} > 0$;
(ii) $d_1a_{22} + d_2a_{11} > 2\sqrt{d_1d_2 \det(J)}$.

The Turing instability (or bifurcation), mathematically speaking, as $d_1 \ll d_2$, occurs when $\mathrm{Im}(\lambda(k)) = 0$, $\mathrm{Re}(\lambda(k)) = 0$ at $k = k_c \neq 0$ [16,50,51]. We adopt the demographic reproductive number R_d in model (5) as the bifurcation parameter and the other parameters as constants and fixed. Then the Turing bifurcation of model (5) occurs when

$$R_{d_T} = \frac{d_1(2R_0^2 - 3R_0 + 1) + d_2(4R_0 + 2\nu - R_0^2 - R_0\nu - 3) - 2P(R_0 - 1)}{d_2R_0\nu}, \tag{36}$$

where $P = \sqrt{d_1R_0(d_1R_0 + 2d_2 - d_2R_0 - d_2\nu - d_1)}$. And the Turing instability takes place for $R_d < R_{dT}$.

The wave-number k_c satisfies

$$k_c = \sqrt{\frac{d_1(1 - R_0) + d_2(4R_0 + 2\nu - R_0^2 - R_0R_d\nu - R_0\nu - 3)}{2d_1d_2R_0}}. \tag{37}$$

In Fig. 3, we show the Turing bifurcation diagram in R_0–R_d plane for model (5) by taking $\nu = 0.15$, $d_1 = 0.01$, $d_2 = 0.25$. The Turing bifurcation curve and the critical boundary line of the positive equilibrium condition separate the parametric space into three domains. In domain I, located above the Turing bifurcation curve, the steady state is only stable solution of the model. In domain III, below the critical boundary line $R_d^+ = \frac{R_0+\nu-1}{\nu R_0}$ of the positive equilibrium condition, there is no positive equilibrium. For parameters in domain II, below the Turing bifurcation curve R_{d_T} and above the critical boundary line of the positive equilibrium condition R_d^+, the corresponding solution of the model is unstable, and Turing instability occurs, therefore Turing patterns emerge. This domain is called the "Turing space". We will focus on the Turing pattern formation for parameters in such a domain.

We plot in Fig. 4 the dispersion relation corresponding to several values of bifurcation parameter R_d while keeping the others fixed as $R_0 = 1.17$, $\nu = 0.15$, $d_1 = 0.01$, $d_2 = 0.25$. In Fig. 4, line (b) corresponds to the critical Turing value $R_{d_T} = 1.77331539$. When $R_d = 1.85 > R_{d_T}$ (e.g., line (a) in Fig. 4), the Turing instability occurs, while $R_d = 1.7 < R_{d_T}$ (e.g., line (c) in Fig. 4), the Turing instability decays. That is to say, when $R_d < R_{d_T}$, the steady state is the only stable solution of model (6).

3. Turing pattern formation

3.1. Numerical techniques

In this section, we perform extensive numerical simulations of the spatially extended model (5) in 2-dimensional spaces, and the qualitative results as well. All our numerical simulations employ the non-zero initial and zero-flux boundary

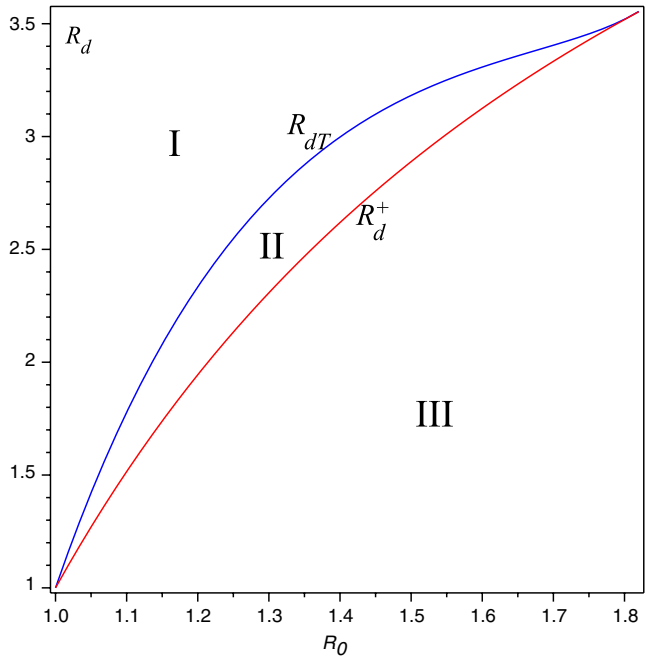

Fig. 3. Turing bifurcation diagram for model (5) using R_0 and R_d as parameters. R_{d_T} is the critical value of the Turing bifurcation, $R_d^+ = \frac{R_0+\nu-1}{\nu R_0}$ is the critical condition of the positive equilibrium. Other parameters are taken as $\nu = 0.15,\ d_1 = 0.01,\ d_2 = 0.25$. Domain II is called the "Turing space".

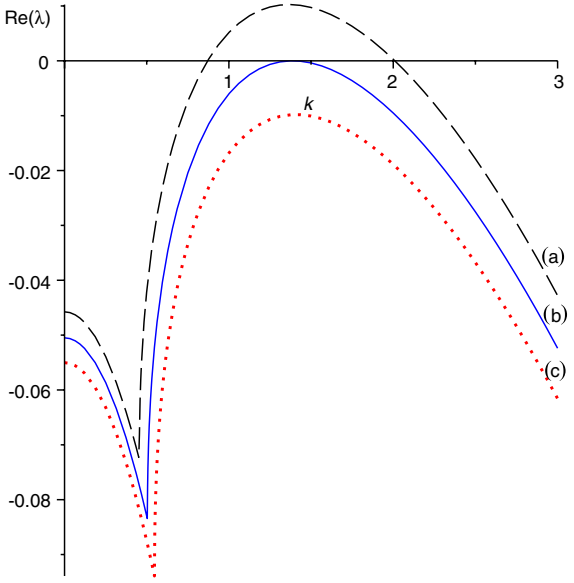

Fig. 4. Variation of dispersion relation of model (5) with $R_0 = 1.17$, $\nu = 0.15,\ d_1 = 0.01,\ d_2 = 0.25$. (a) $R_d = 1.85$; (b) R_{d_T}, the Turing instability occurs; (c) $R_d = 1.7$, the Turing instability decays.

conditions (i.e., Eqs. (6) and (7)) with a system size of $L \times L$, with $L = 200$ discretized through $x \to (x_0, x_1, x_2, \ldots, x_N)$ and $y \to (y_0, y_1, y_2, \ldots, y_N)$, with $N = 600$. We take the time steps size $\tau = \frac{1}{40}$, other parameters are fixed as $\nu = 0.15, R_d = 2, d_2 = 0.25$.

We use the standard five-point approximation for the 2D Laplacian with the zero-flux boundary conditions. More precisely, the concentrations $(S_{i,j}^{n+1}, I_{i,j}^{n+1})$ at the moment $(n+1)\tau$ at the mesh position (x_i, y_j) are given by

$$S_{i,j}^{n+1} = S_{i,j}^n + \tau d_1 \Delta_h S_{i,j}^n + \tau f(S_{i,j}^n, I_{i,j}^n),$$
$$I_{i,j}^{n+1} = I_{i,j}^n + \tau d_2 \Delta_h I_{i,j}^n + \tau g(S_{i,j}^n, I_{i,j}^n),$$

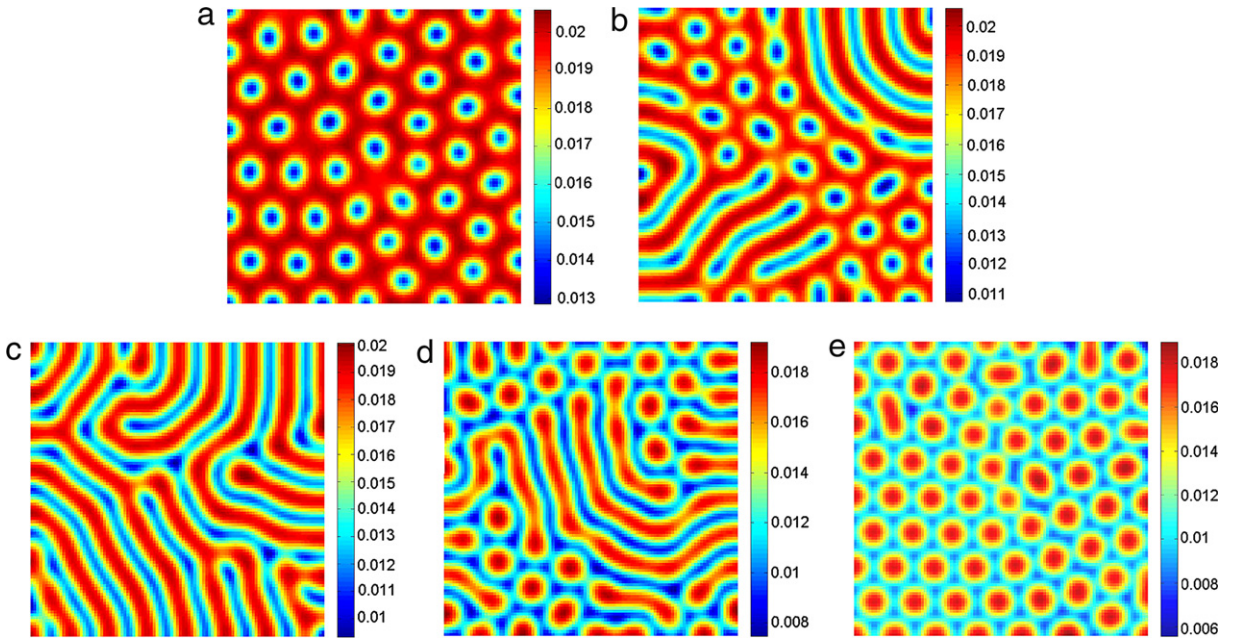

Fig. 5. The five categories of Turing patterns of I in model (5) with parameters $R_d = 2.0$, $\nu = 0.15$, $d_1 = 0.01$, $d_2 = 0.25$. (a) $R_0 = 1.14$; (b) $R_0 = 1.154$; (c) $R_0 = 1.17$; (d) $R_0 = 1.2$; (e) $R_0 = 1.213$. Times: (a)–(d) 3750; (e) 7500.

with the Laplacian defined by

$$\Delta_h S^n_{i,j} = \frac{S^n_{i+1,j} + S^n_{i-1,j} + S^n_{i,j+1} + S^n_{i,j-1} - 4S^n_{i,j}}{h^2},$$

where $f(S, I)$ and $g(S, I)$ are defined as Eq. (5), and $h = \frac{L}{N} = \frac{1}{3}$.

Initially, the entire system is placed at the stationary state (S^*, I^*), and the propagation velocity of the initial perturbation is thus on the order of 5×10^{-4} space units per time unit. The system is then integrated for 1×10^5 or 3×10^5 time steps and some images recorded. After the initial period during which the perturbation spreads, either the system goes into a time dependent state, or to an essential steady state (time independent).

In the numerical simulations, different types of dynamics are observed and we have found that the distributions of susceptible and infectious are always of the same type. Consequently, we will restrict our analysis of pattern formation to one distribution. In this section, we show the distribution of infectious I, for instance.

3.2. The categories of Turing patterns

Now, we show the patterns for the different values of R_0 and R_d located in the "Turing space" (the domain II in Fig. 3).

In Fig. 5, by numerical simulations, we show five categories of Turing patterns for the distribution of infectious I of model (5) arising from random initial conditions for several values of R_0.

Pattern-a, $R_0 = 1.14$, consists of blue (minimum density of I) hexagons on a red (maximum density of I) background, i.e., the infectious are isolated zones with low population density. We call this pattern "holes" (Fig. 5(a)).

Pattern-b, $R_0 = 1.154$, a few stripes emerge, and the remainder of the holes pattern remains time independent, i.e., stripes–holes pattern (Fig. 5(b)).

When R_0 is increased to 1.17, model dynamics exhibits a transition from stripes–holes growth to stripes replication, i.e., holes decay and the stripes pattern emerges, c.f., Pattern-c (Fig. 5(c)).

In Pattern-d, $R_0 = 1.2$, a few red hexagons (i.e., spots, associated with high population densities of I) fill in the stripes, i.e., the stripes–spots pattern emerges (Fig. 5(d)).

And while R_0 is increased to 1.212, model dynamics exhibits a transition from stripe-spots growth to spots replication, i.e., stripes decay and the spots pattern emerges, c.f., Pattern-e (Fig. 5(e)).

From Fig. 5, one can see that for the fixed $R_d = 2.0$, on increasing the control parameter R_0, the sequence "holes → hole-stripe mixtures → stripes → spot-stripe mixtures → spots" is observed.

From the view of epidemic dynamics, in Fig. 5(a), Pattern-a, one can see that there exists the "holes" pattern replication—the infectious I is the isolated zone with low density, and the remainder region is of high density, which is larger than the "holes" region. That's to say, under the control of these parameters, the epidemic may break out in the area. In the case of Fig. 6(e), Pattern-e, the infectious I is the isolated zones with high density, the remainder region is of low density, which

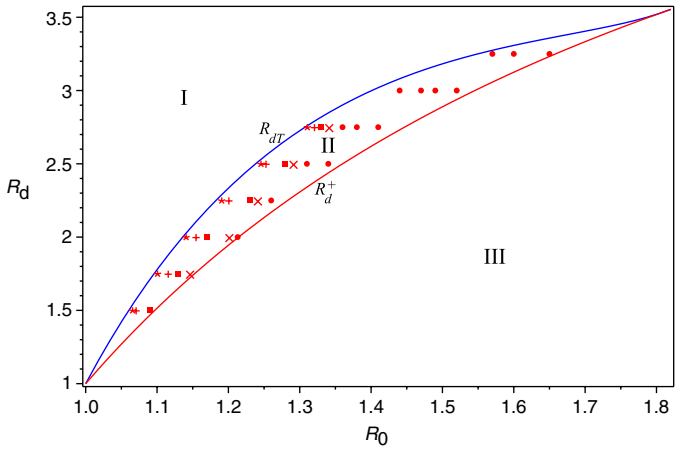

Fig. 6. The map of the Turing patterns in the "Turing space". The signs indicate the location in parameter space where the patterns in Fig. 5 were found. ★ -Pattern-a; + -Pattern-b; ■ -Pattern-c; × -Pattern-d; ● -Pattern-e.

means the epidemic may not break out in the area. In other words, in this case, the area is safe. The epidemic significance of the other cases, Pattern-b, Pattern-c and Pattern-d, can be determined in the same way as the above two cases.

3.3. The map of the Turing patterns in the Turing space

In the above subsection, we show all five categories Turing patterns in Fig. 5. We are interested in the distributions of the Turing patterns in the Turing space. In Fig. 6, we show the map of the Turing patterns in the Turing space.

One can view Fig. 6 as a map and Fig. 5 as the key to the map. In Fig. 6, the five categories of Turing patterns illustrated in Fig. 5 are designated by signs "★, +, ■, ×, ●", respectively. In Fig. 6, the signs indicate the pattern found at that point in the Turing space.

From Fig. 6, we can be sure that when $R_d < 2$, spots pattern cannot be found, but we can observe the holes pattern, which means that the epidemic may break out in the area. While $R_0 \geq 1.36$, the model dynamics only exhibits spots pattern replication, which means that the epidemic may not break out. In other words, in this case, the area is safe.

3.4. The evolutionary processes of Turing pattern formation

In the Turing pattern formation, there are three categories of patterns which are basic, they are holes (this pattern is called "H_π"-pattern), stripes and spots (this pattern is called "H_0"-pattern, too). Next, we show the evolutionary processes of Turing pattern formation of these three patterns. As an example, we adopt the parameters as $R_d = 2.0$, $\nu = 0.15$, $d_1 = 0.01$, $d_2 = 0.25$.

In Fig. 7, $R_0 = 1.14$. There exhibits a competition between stripes and spots. The pattern takes a long time to settle down, starting with a homogeneous state $E^* = (0.1333743716, 0.01867241203)$ (c.f., Fig. 7(a)), and the random perturbations lead to the formation of stripes and spots (c.f., Fig. 7(b)), and ending with holes only (c.f., Fig. 7(d))—the infectious are isolated zones with low population density, which is time-independent. In this case, one can see that the diseases' spread is getting bigger with time increasing.

In Fig. 8, $R_0 = 1.17$, starting with a homogeneous state $E^* = (0.07548640028, 0.01283268805)$, the random perturbations lead to the formation of stripes–holes (c.f., Fig. 8(b)), and the later random perturbations make these holes decay, ending with the time-independent stripes pattern (c.f., Fig. 8(d)).

In Fig. 9, $R_0 = 1.212$, $E^* = (0.003630726111, 0.0007697139352)$. The random perturbations lead to the formation of stripes–holes (c.f., Fig. 9(b)), and the later random perturbations make these holes decay, ending with the time-independent spots pattern (c.f., Fig. 9(d))—the infectious are isolated zones with high population density. In this case, one can see that the diseases' spread is getting smaller with time increasing.

For the sake of further learning about these evolutionary processes, in Fig. 10, as an example, we take the position $(x, y) = (50, 50)$ in the spatial domain $\Omega = [0, 100] \times [0, 100]$, the solutions to which in the spatial model (6) illustrate the time-series plots for S and I, corresponding to the holes and spots patterns in Figs. 7 and 9, respectively.

From Fig. 10(a), $R_0 = 1.14$, one can see that, when $t > 2000$, $S \in (0.165, 0.170)$ and $I \in (0.0194, 0.0196)$. While in Fig. 10(b), $R_0 = 1.17$, when $t > 2000$, $S \in (0.198, 0.202)$ and $I \in (0.016, 0.018)$. That's to say, when R_0 increase from 1.14 to 1.212, the value of susceptible S will increase and I decrease. This means that the diseases' spread is getting smaller with R_0 increasing.

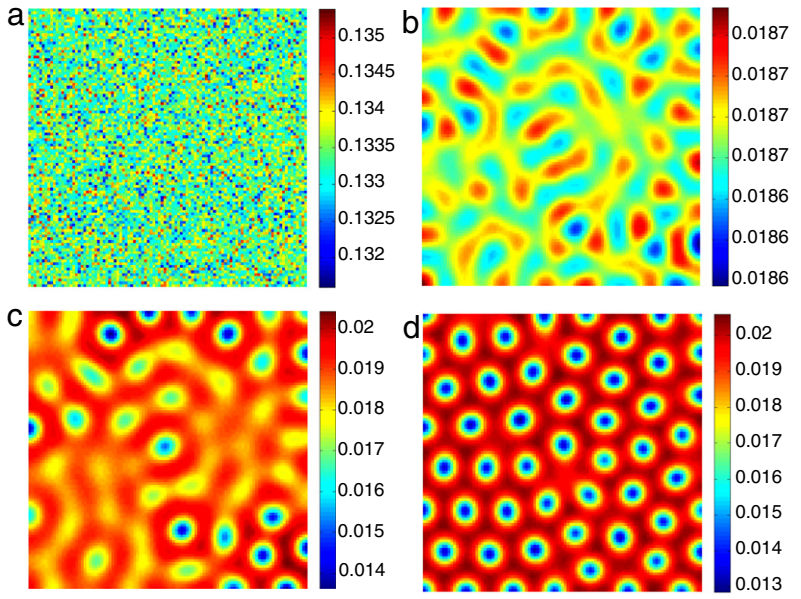

Fig. 7. Holes pattern formation for model (5) by taking $R_0 = 1.14$, $R_d = 2.0$, $\nu = 0.15$, $d_1 = 0.01$, $d_2 = 0.25$. Times: (a) 0; (b) 500; (c) 1500; (d) 3750.

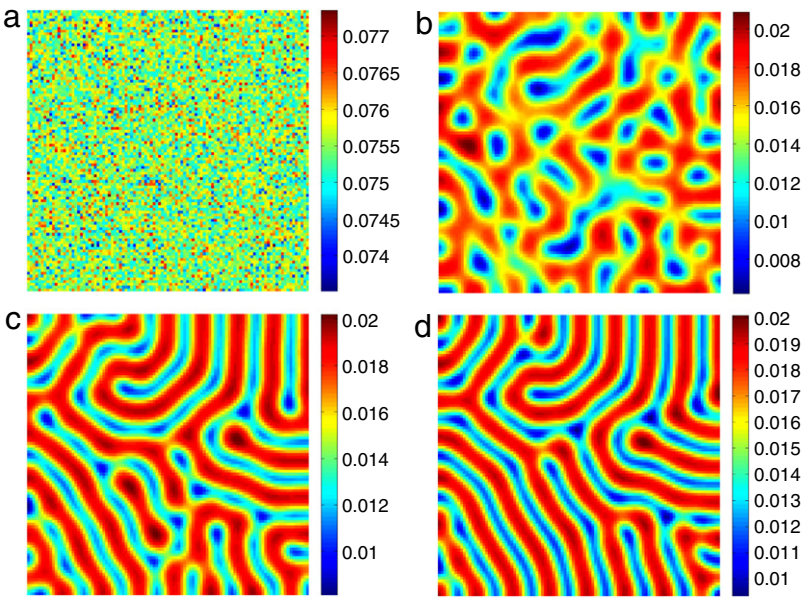

Fig. 8. Stripes pattern formation for model (5) by taking $R_0 = 1.17$, $R_d = 2.0$, $\nu = 0.15$, $d_1 = 0.01$, $d_2 = 0.25$. Times: (a) 0; (b) 250; (c) 1000; (d) 3750.

4. The disease spreading with the varying diffusion

In general, diffusion is a transport of the concentrations from a region of higher concentration to one of lower concentration by random motion [13]. For an epidemic model such as model (5), there may be some reasons to make diffusion vary for susceptible S or infectious I. In this section, we will focus on the disease spreading with the varying diffusion.

4.1. Fixed d_2, disease spreading with the varying d_1

In the first case, we will consider the spatiotemporal dynamics of model (5) with fixed parameters $R_0 = 1.2$, $R_d = 2.0$, $d_2 = 0.25$. The Turing patterns and the corresponding time-series plots are shown in Fig. 11. In the below panel, we

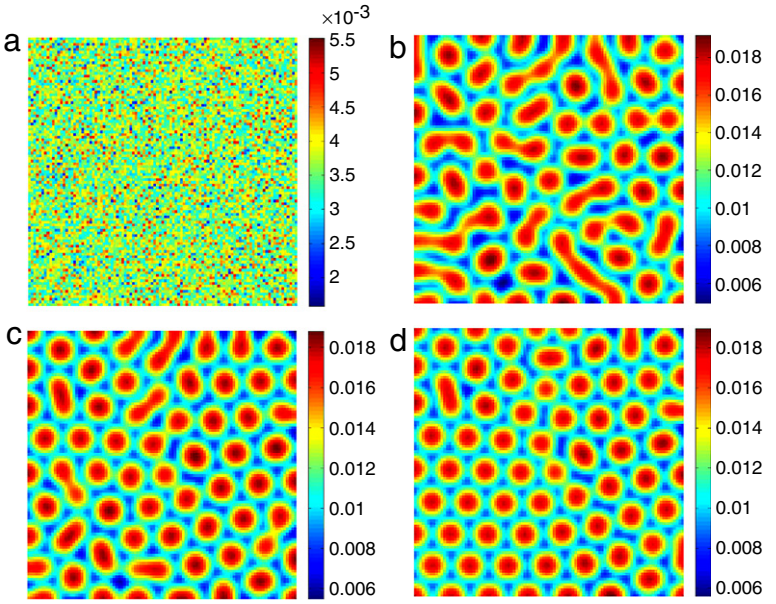

Fig. 9. Spots pattern formation for model (5) by taking $R_0 = 1.212$, $R_d = 2.0$, $\nu = 0.15$, $d_1 = 0.01$, $d_2 = 0.25$. Times: (a) 0; (b) 500; (c) 1500; (d) 7500.

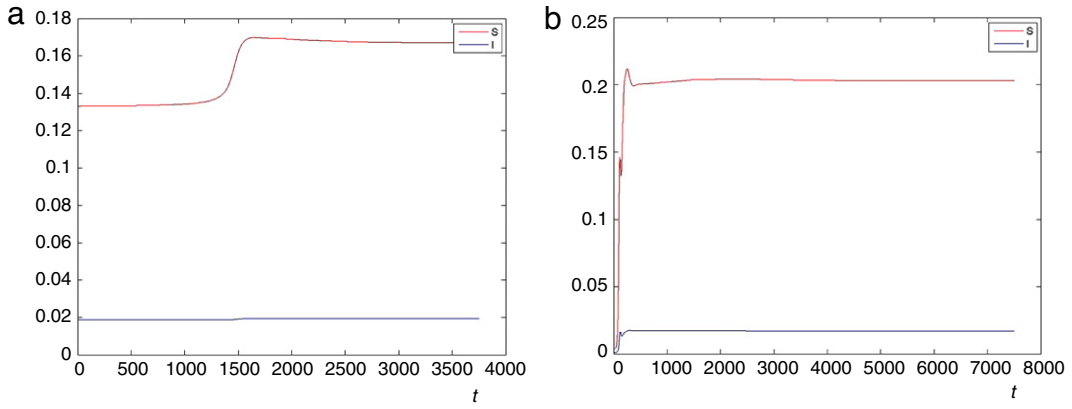

Fig. 10. Time-series plots for model (5) by taking $R_d = 2.0$, $\nu = 0.15$, $d_1 = 0.01$, $d_2 = 0.25$ and (a) $R_0 = 1.14$; (b) $R_0 = 1.212$.

take the position $(x, y) = (50, 50)$ in the spatial domain $\Omega = [0, 100] \times [0, 100]$, the solutions to which in the spatial model (6) illustrate the time-series plots for S and I.

From the above panel of Fig. 11, one can see that when d_1 varies from 0.01 to 0.075, there is a sequence "spots–stripes→ spots → spots–stripes" pattern that can be observed. From the below panel of Fig. 11, in the same varying diffusion d_1, one can see that, when $t > 1000$, with $d_1 = 0.01$, $S \in (0.14, 0.18)$ and $I \in (0.014, 0.016)$; while $d_1 = 0.05$, $S \in (0.055, 0.075)$ and $I \in (0.008, 0.011)$; and $d_1 = 0.075$, $S \in (0.015, 0.022)$ and $I \in (0.0036, 0.0044)$. That's to say, the value of I will decrease along with the increasing of d_1. Similar to the value of S.

4.2. Fixed d_1, disease spreading with the varying d_1

Next, we will consider the spatiotemporal dynamics of model (5) with fixed parameters $R_0 = 1.2$, $R_d = 2.0$, $d_1 = 0.03$, and the Turing patterns and the corresponding time-series plots are shown in Fig. 12. From the above panel of Fig. 12, one can see that when d_1 vary from 0.01 to 0.075, there is a sequence "spots→ spots–stripes→stripes" pattern that can be observed. From the below panel of Fig. 12, in the same varying diffusion d_1, one can see that, when $t > 1000$, with $d_2 = 0.25$, $S \in (0.025, 0.03)$ and $I \in (0.007, 0.008)$; while $d_2 = 0.75$, $S \in (0.01, 0.02)$ and $I \in (0.009, 0.011)$; and $d_2 = 1.0$, $S \approx 0.01$, $I \approx 0.011$ and $S < I$. That's to say, the value of S will decrease along with the increasing of d_2. In contrast, the value of I will increase along with the increasing of d_2.

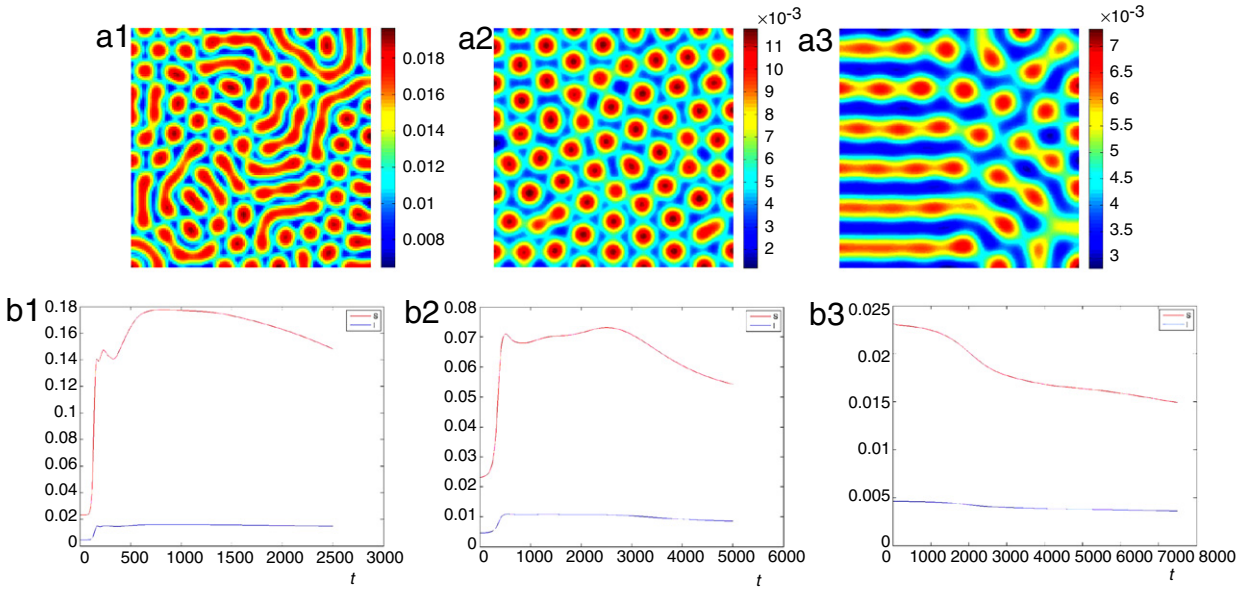

Fig. 11. Spatiotemporal dynamics of varying d_1. (a) Turing patterns; (b) time-series plots. (1) $d_1 = 0.01$; (2) $d_1 = 0.05$; (3) $d_1 = 0.075$.

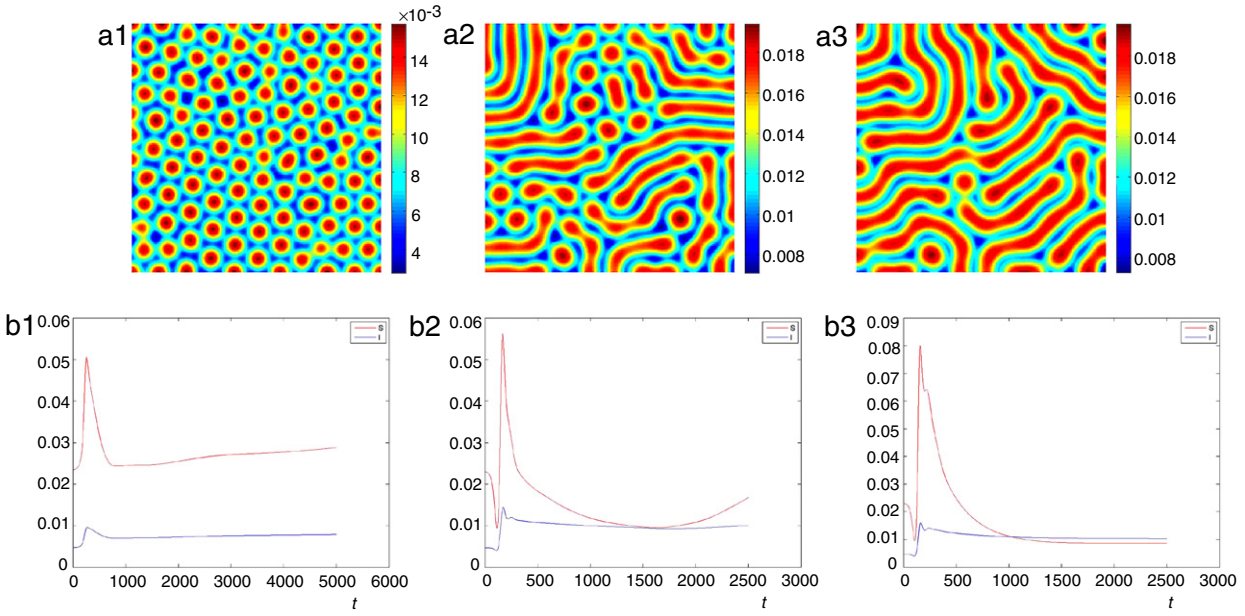

Fig. 12. Spatiotemporal dynamics of varying d_2. (a) Turing patterns; (b) time-series plots. (1) $d_2 = 0.25$; (2) $d_2 = 0.75$; (3) $d_2 = 1.0$.

5. Conclusions and remarks

In this paper, we extend to consider and analyze a reaction–diffusion epidemic model with demographic and epidemiological processes under the zero-flux boundary conditions. Three re-parameterized quantities, the basic demographic reproductive number (R_d), the basic epidemiological reproductive number (R_0) and the ratio (ν) between the average life spans of susceptible and infective class are utilized in its qualitative analysis. The spatial model (5) is introduced in a general form so that it has broad applications to a range of interaction populations.

The value of this study lies in three aspects. First, it presents global stability of the equilibria and the analysis of Turing bifurcation, which determines the Turing space in the spatial domain. Second, it illustrates five categories of Turing patterns close to the onset Turing bifurcation via numerical simulations, from which one can be sure of the parametric range for epidemic outbreak or safety in the spatial domain. Third, it shows the relations between the Turing patterns and diffusion with diseases spreading.

In our numerical simulation, we demonstrate that there exists a range of values in (R_0, R_d) parameter space where different spatial patterns emerge. Our conclusions can be compared with those in [39–42]. In [39], the authors investigated an epidemic model with constant rate of removal of the infectives, and get a stripes pattern and a spots–stripes mixture pattern, but no spots pattern of the epidemic model. In [40], the authors considered an $S-I$ model with nonlinear incidence rate, and got a spots–stripes and spots pattern (we call these "spots" patterns "holes" in this paper). In [41], the authors indicated that the chaos pattern can emerge in the spatial epidemic model. Our results show that the model dynamics exhibits a richer and complex pattern replication: for the fixed R_d, on increasing the control parameter R_0, the sequence "holes → hole-stripe mixtures → stripes → spot-stripe mixtures → spots" is observed. And with the "holes" pattern, the epidemic may be an outbreak in the region, while with the "spots" pattern, the epidemic may not be an outbreak in the region.

On the other hand, we focus on the complex dynamics of diseases spreading with the basic reproduction number R_0 and the diffusion-varying d_1, d_2. We find that the diseases' spread is getting smaller with R_0 increasing. And with fixed d_2, the value of I will decrease along with the increasing of d_1; while with fixed d_1, the value of I will increase along with the increasing of d_2. That's to say, the increasing diffusion d_2 will increase the speed of diseases spreading. In other words, our result may be a new answer to the question: "Which is better, isolation from the infectious or not?" That is, isolation is better.

In the present paper, we adopt the Laplacian operator $\nabla^2 = \frac{\partial^2}{\partial x^2} + \frac{\partial^2}{\partial y^2}$ to approximate the diffusive process, i.e., the diffusion of the species S and I is random in xy plane. But this is not necessarily the case, however. From a biological perspective, the diffusion of individuals may be connected with other things, such as searching for food, escaping high infection risks, migrating controlled by the climate and others. In these cases, individuals tend to diffuse in the direction of lower density of a population to obtain richer resources, or move along the gradient of infectious individuals to avoid higher infection, etc.. We think the process of diffusion in the epidemic system with other mathematical methods may be modeled. This is desirable in future studies.

The methods and results in the present paper may enrich the research of pattern formation in the epidemic model and may well explain the filed observations in some areas.

Acknowledgments

The authors would like to thank Prof. Huaiping Zhu (York University) for a careful reading of the manuscript and insightful suggestions which helped us to improve the manuscript. This research was supported by the National Science Foundation of China (31070322) and the State Key Laboratory of Vegetation and Environmental Change.

References

[1] W.O. Kermack, A.G. McKendrick, A contribution to the mathematical theory of epidemics, Proc. R. Soc. A 115 (1927) 700–721.
[2] Z. Ma, Y. Zhou, J. Wu, Modeling and Dynamics of Infectious Diseases, Higher Education Press, Beijing, 2009.
[3] H.L. Smith, Subharmonic bifurcation in an SIR epidemic model, J. Math. Biol. 17 (2) (1983) 163–177.
[4] E. Beretta, Y. Takeuchi, Global stability of an SIR epidemic model with time delays, J. Math. Biol. 33 (3) (1995) 250–260.
[5] H.W. Hethcote, The mathematics of infectious diseases, SIAM Rev. 42 (4) (2000) 599–653.
[6] M. Fan, M.Y. Li, K. Wang, Global stability of an SEIS epidemic model with recruitment and a varying total population size, Math. Biosci. 170 (2) (2001) 199–208.
[7] M.Y. Li, H.L. Smith, L. Wang, Global dynamics of an SEIR epidemic model with vertical transmission, SIAM J. Appl. Math. 62 (1) (2001) 58–69.
[8] S. Ruan, W. Wang, Dynamical behavior of an epidemic model with a nonlinear incidence rate, J. Differential Equations 188 (1) (2003) 135–163.
[9] F. Berezovsky, G. Karev, B. Song, C. Castillo-Chavez, A simple epidemic model with surprising dynamics, Math. Biosci. Eng. 2 (2005) 133–152.
[10] W. Wang, S. Ruan, Bifurcations in an epidemic model with constant removal rate of the infectives, J. Math. Anal. Appl. 291 (2) (2004) 775–793.
[11] Y. Zhou, Z. Ma, F. Brauer, A discrete epidemic model for SARS transmission and control in China, Math. Comp. Model. 40 (13) (2004) 1491–1506.
[12] D. Xiao, S. Ruan, Global analysis of an epidemic model with nonmonotone incidence rate, Math. Biosci. 208 (2) (2007) 419–429.
[13] A. Okubo, S. Levin, Diffusion and Ecological Problems: Modern Perspectives, second ed., Springer, New York, 2001.
[14] C. Neuhauser, Mathematical challenges in spatial ecology, Notices Amer. Math. Soc. 48 (11) (2001) 1304–1314.
[15] R. Cantrell, C. Cosner, Spatial Ecology via Reaction–Diffusion Equations, Wiley, 2003.
[16] J.D. Murray, Mathematical Biology, third ed., Springer, New York, 2003.
[17] E.E. Holmes, M.A. Lewis, J.E. Banks, R.R. Veit, Partial differential equations in ecology: spatial interactions and population dynamics, Ecology 75 (1994) 17–29.
[18] L. Rass, J. Radcliffe, Spatial Deterministic Epidemics, American Mathematical Society, 2003.
[19] Y. Hosono, B. Ilyas, Traveling waves for a simple diffusive epidemic model, Math. Model. Method. Appl. Sci. 5 (1995) 935–966.
[20] I. Cruickshank, W. Gurney, A. Veitch, The characteristics of epidemics and invasions with thresholds, Theor. Popu. Biol. 56 (3) (1999) 279–292.
[21] N.M. Ferguson, C.A. Donnelly, R.M. Anderson, The foot-and-mouth epidemic in Great Britain: pattern of spread and impact of interventions, Science 292 (5519) (2001) 1155.
[22] B.T. Grenfell, O.N. Bjornstad, J. Kappey, Travelling waves and spatial hierarchies in measles epidemics, Nature 414 (6865) (2001) 716–723.
[23] D. He, L. Stone, Spatio-temporal synchronization of recurrent epidemics, Proc. R. Soc. Lond. B 270 (1523) (2003) 1519–1526.
[24] A.L. Lloyd, V.A. Jansen, Spatiotemporal dynamics of epidemics: synchrony in metapopulation models, Math. Biosci. 188 (1–2) (2004) 1–16.
[25] W.M. van Ballegooijen, M.C. Boerlijst, Emergent trade-offs and selection for outbreak frequency in spatial epidemics, PNAS 101 (52) (2004) 18246.
[26] J.A.N. Filipe, M.M. Maule, Effects of dispersal mechanisms on spatio-temporal development of epidemics, J. Theoret. Biol. 226 (2) (2004) 125–141.
[27] G. Funk, V. Jansen, S. Bonhoeffer, T. Killingback, Spatial models of virus-immune dynamics, J. Theoret. Biol. 233 (2) (2005) 221–236.
[28] M. Pascual, F. Guichard, Criticality and disturbance in spatial ecological systems, TREE 20 (2) (2005) 88–95.
[29] N.V. Festenberg, T. Gross, B. Blasius, Seasonal forcing drives spatio-temporal pattern formation in rabies epidemics, Math. Model. Nat. Phen. 2 (4) (2007) 63–73.
[30] G. Mulone, B. Straughan, W. Wang, Stability of epidemic models with evolution, Studies in Appl. Math. 118 (2) (2007) 117–132.
[31] F.M. Hilker, M. Langlais, S.V. Petrovskii, H. Malchow, A diffusive SI model with Allee effect and application to FIV, Math. Biosci. 206 (1) (2007) 61–80.

[32] K. Wang, W. Wang, Propagation of HBV with spatial dependence, Math. Biosci. 210 (1) (2007) 78–95.
[33] K. Wang, W. Wang, S. Song, Dynamics of an HBV model with diffusion and delay, J. Theoret. Biol. 253 (1) (2008) 36–44.
[34] H. Malchow, S.V. Petrovskii, E. Venturino, Spatiotemporal Patterns in Ecology and Epidemiology—Theory, Models, and Simulation, in: Mathematical and Computational Biology Series, Chapman & Hall/CRC, Boca Raton, 2008.
[35] R.K. Upadhyay, N. Kumari, V. Rao, Modeling the spread of bird flu and predicting outbreak diversity, Nonl. Anal.: RWA 9 (4) (2008) 1638–1648.
[36] R. Xu, Z. Ma, An HBV model with diffusion and time delay, J. Theoret. Biol. 257 (3) (2009) 499–509.
[37] B. Camara, Complexité de dynamiques de modèles proie-prédateur avec diffusion et applications, Ph.D Thesis, Lorient, Universitè du Havre, 2009.
[38] A.M. Turing, The chemical basis of morphogenesis, Phil. Trans. Roy. Soc. Lond. B 237 (641) (1952) 37–72.
[39] Q. Liu, Z. Jin, Formation of spatial patterns in an epidemic model with constant removal rate of the infectives, J. Stat. Mech. 2007 (2007) P05002.
[40] G. Sun, Z. Jin, Q.X. Liu, L. Li, Pattern formation in a spatial *S–I* model with non-linear incidence rates, J. Stat. Mech. 2007 (2007) P11011.
[41] G. Sun, Z. Jin, Q.X. Liu, L. Li, Chaos induced by breakup of waves in a spatial epidemic model with nonlinear incidence rate, J. Stat. Mech. 2008 (2008) P08011.
[42] G. Sun, Z. Jin, Q.X. Liu, L. Li, Spatial pattern in an epidemic system with cross-diffusion of the susceptible, J. Biol. Sys. 17 (1) (2009) 1–12.
[43] Y. Cai, W. Wang, Spatiotemporal dynamics of a reaction–diffusion epidemic model with nonlinear incidence rate, J. Stat. Mech. (2011) P02025.
[44] W. Wang, Y. Lin, H. Wang, H. Liu, Y. Tan, Pattern selection in an epidemic model with self and cross diffusion, J. Biol. Sys. 19 (2011) 19–31.
[45] M. Bendahmane, M. Saad, Mathematical analysis and pattern formation for a partial immune system modeling the spread of an epidemic disease, Acta Appl. Math. 115 (2011) 17–42.
[46] P. Arcuri, J.D. Murray, Pattern sensitivity to boundary and initial conditions in reaction–diffusion models, J. Math. Biol. 24 (2) (1986) 141–165.
[47] T.W. Hwang, Y. Kuang, Deterministic extinction effect of parasites on host populations, J. Math. Biol. 46 (1) (2003) 17–30.
[48] W. Chen, M. Wang, Qualitative analysis of predator–prey models with Beddington–DeAngelis functional response and diffusion, Math. Comput. Model. 42 (1–2) (2005) 31–44.
[49] D. Henry, Geometric theory of semilinear parabolic equations, in: Lecture Notes in Mathematics, Springer-Verlag, 1981.
[50] M. Baurmann, T. Gross, U. Feudel, Instabilities in spatially extended predator–prey systems: spatio-temporal patterns in the neighborhood of Turing–Hopf bifurcations, J. Theoret. Biol. 245 (2) (2007) 220–229.
[51] W. Wang, Q. Liu, Z. Jin, Spatiotemporal complexity of a ratio-dependent predator–prey system, Phys. Rev. E 75 (5) (2007) 051913.